http://www.pjbs.org



ISSN 1028-8880

Pakistan Journal of Biological Sciences



Asian Network for Scientific Information 308 Lasani Town, Sargodha Road, Faisalabad - Pakistan

ISSN 1028-8880 DOI: 10.3923/pjbs.2025.505.522



Research Article

Discovery of Potent Antibacterial and Anticancer Flavonoids from Beehive-Associated *Streptomyces griseoaurantiacus* HNF214

¹Thongchai Taechowisan, ¹Thanaporn Chuen-Im and ²Waya S. Phutdhawong

Abstract

Background and Objective: Actinomycetes from beehives are a potential source of bioactive compounds. This study aimed to isolate actinomycetes from *Apis florea* beehives, characterize their compounds and evaluate their antibacterial and anticancer properties, including underlying mechanisms. **Materials and Methods:** Actinomycetes were isolated from *Apis florea* beehives in Nakhon Pathom, Thailand. The most active isolate, HNF214, was identified by 16S rRNA gene sequencing and characterized morphologically. Bioactive compounds were extracted, purified and identified using spectroscopy. Antibacterial (MIC/MBC) and anticancer (MTT assay on various cell lines) activities were tested. Molecular docking predicted interactions with MEK1/MEK2 and *in silico* ADMET properties were assessed. ERK1/2 phosphorylation was measured by ELISA. One-way ANOVA and Tukey's *post hoc* test were employed, with significance defined as p<0.05. **Results:** Thirty-two isolates yielded *Streptomyces griseoaurantiacus* HNF214, which showed potent antibacterial activity against Gram-positive bacteria. Two compounds, quercetin and isoquercetin, were purified. They demonstrated significant cytotoxicity against breast, cervical and liver cancer cells (IC₅₀ 234-811 μg/mL) with lower toxicity to normal cells. Docking revealed favorable binding to MEK1/MEK2 and ELISA confirmed reduced ERK1/2 phosphorylation. The ADMET predictions were mostly favorable, but compound 1 showed potential carcinogenicity/mutagenicity. **Conclusion:** *Streptomyces griseoaurantiacus* HNF214 from beehives produces quercetin and isoquercetin, exhibiting both antibacterial and anticancer activities, likely via MAPK/ERK pathway inhibition. While promising, further safety and *in vivo* studies are crucial before therapeutic development.

Key words: Antibacterial activity, anticancer activity, beehive, flavonoids, Streptomyces griseoaurantiacus HNF214

Citation: Taechowisan, T., T. Chuen-Im and W.S. Phutdhawong, 2025. Discovery of potent antibacterial and anticancer flavonoids from beehive-associated *Streptomyces griseoaurantiacus* HNF214. Pak. J. Biol. Sci., 28: 505-522.

Corresponding Author: Thongchai Taechowisan, Department of Microbiology, Faculty of Science, Silpakorn University, Nakhon Pathom 73000, Thailand

Copyright: © 2025 Thongchai Taechowisan *et al.* This is an open access article distributed under the terms of the creative commons attribution License, which permits unrestricted use, distribution and reproduction in any medium, provided the original author and source are credited.

Competing Interest: The authors have declared that no competing interest exists.

Data Availability: All relevant data are within the paper and its supporting information files.

¹Department of Microbiology, Faculty of Science, Silpakorn University, Nakhon Pathom 73000, Thailand

²Department of Chemistry, Faculty of Science, Silpakorn University, Nakhon Pathom 73000, Thailand

INTRODUCTION

a widespread group Actinomycetes are of microorganisms known for their exceptional ability to adapt to diverse ecological niches. These environments range from common soil matrices to specialized biological systems such as insect intestinal tracts¹. Within terrestrial environments, actinomycetes are significant contributors to the breakdown of organic matter and the cycling of essential nutrients. Certain species also form mutualistic associations with plants, enabling nitrogen fixation in exchange for plant-derived sugars. Their robust nature allows them to flourish in aquatic environments, including seabeds, estuarine salt marshes, lakes and rivers. Additionally, actinomycetes have been observed inhabiting the gastrointestinal systems of animals, where they are thought to contribute to host digestive functions¹. The broad distribution and ecological versatility of actinomycetes highlight their critical importance in the health and function of numerous ecosystems.

Beyond their ubiquitous environmental presence, actinomycetes are frequently isolated from beehives, showing up in various components such as worker bee tissues, brood cells and other hive materials²⁻⁷. Their consistent occurrence in these apiary environments suggests they might offer advantages for bee health. Significantly, actinomycetes are well-known for producing a wide array of antimicrobial compounds, including antibiotics, which could help protect bee colonies from bacterial pathogens^{6,8}.

The broader group of actinomycetes is extensively documented for its ability to synthesize a diverse range of bioactive compounds, such as antibiotics, enzymes and antifungals. These compounds are thought to be crucial for their survival and their competitive interactions within microbial communities⁹. While the general production of these compounds by actinomycetes is well-established, specific research into isolating and identifying these compounds from beehive-associated actinomycetes is an emerging area. Nevertheless, recent studies have shown promising outcomes. For example, Streptomyces sp., AmelAP-1, recovered from beehive pollen stores, has exhibited inhibitory activity against Paenibacillus larvae, a major bacterial pathogen affecting honey bees. This protective effect has been linked to the production of piceamycin by this Streptomyces strain⁶.

This study aimed to isolate and characterize actinomycetes from *Apis florea* beehives, identify bioactive compounds from the potent strain HNF214 and evaluate their antibacterial, anticancer and cytotoxic properties, supported by molecular docking and ADMET analysis.

MATERIALS AND METHODS

Study area: This research was conducted at Silpakorn University, Nakhon Pathom, Thailand, within the Department of Microbiology and Chemistry. Experimental procedures were carried out from June, 2024 to May, 2025.

Sample collection and actinomycete isolation: Five *Apis florea* beehives were collected from the Rose Garden, Sampran, Nakhon Pathom, Thailand (13.73636 N, 100.24372 E) during June-July 2024. Beekeepers assisted in the collection process. Immediately following collection, samples were sealed in plastic bags to prevent contamination and transported to the laboratory facilities at Silpakorn University.

For the isolation of actinomycetes, 10 g of each sample was added to 90 mL of phosphate-buffered saline (PBS) in a stomacher bag. The samples were then mechanically homogenized for 10 min. One hundred microliters of the resulting suspension were spread onto humic-acid vitamin agar. To suppress the growth of undesirable microorganisms, the agar was supplemented with cycloheximide (50 μ g/mL) and nalidixic acid (20 μ g/mL). Plates were incubated at 32°C for 2 weeks. Presumptive actinomycete colonies were identified visually based on their characteristic morphological features. Purified colonies were subsequently subcultured onto International *Streptomyces* project medium 2 (ISP-2) for further propagation and characterization ¹⁰.

Screening of antibacterial actinomycetes and bioactive compound extraction: A total of 32 actinomycete isolates were evaluated for their antimicrobial properties against a panel of bacterial strains: *Bacillus cereus* TISTR687, *Bacillus subtilis* TISTR008, *Staphylococcus aureus* TISTR885, *Staphylococcus epidermidis* TISTR518 and a clinical isolate of methicillin-resistant *Staphylococcus aureus* (MRSA) Sp3. The screening procedure followed a method described by Taechowisan *et al.*¹¹, with antimicrobial activity assessed using a slightly modified soft-agar overlay technique¹². Inhibition zones were observed and measured and all experiments were performed in triplicate.

Among the tested isolates, strain HNF214 demonstrated the most potent antibacterial activity. This strain was subsequently identified through a combination of morphological, physiological and chemotaxonomic characterizations, as per the methodologies established by Cassarini *et al.*¹³.

For the extraction of metabolites, strain HNF214 was cultured on 750 Petri dishes containing ISP-2 agar (total volume 15 L) and incubated at 32°C for 21 days. Bioactive

compounds were extracted using a modified protocol based on Taechowisan *et al.*¹⁴. The cultured agar medium was cut into small pieces and then extracted three times with 15 L of ethyl acetate. The pooled organic solvent was concentrated to dryness using rotary evaporation, yielding 18.75 g of a dark brown solid. Thin-layer chromatography-direct bioautography (TLC-DB) was performed according to the methods described by Jesionek *et al.*¹⁵.

The resulting crude extract was divided into two portions. Part 1 was resuspended in 5 mL of sterile Dimethyl Sulfoxide (DMSO) to achieve an initial concentration of 10.24 mg/mL. This portion was stored at -20°C until further testing for antibacterial and anticancer activities. Part 2 was resuspended in dichloromethane (CH₂Cl₂) and reserved for subsequent compound purification and characterization.

Identification of the selected strain: Strain HNF214 was selected for comprehensive identification. Morphological characteristics were observed following 15 days of incubation on ISP-2 medium. These observations included the presence of aerial mycelium, spore mass color, distinct reverse colony color, production of diffusible pigments and the morphology of sporophores and spore chains. For chemotaxonomic analysis, diaminopimelic acid isomers and sugars from whole-cell extracts were analyzed using established methodologies^{16,17}.

Scanning electron microscopy: The morphology of the chosen strain was further examined using Scanning Electron Microscopy (SEM). Sample preparation adhered to the methods described by Castillo *et al.*¹⁸. Prepared samples underwent critical point drying with liquid CO₂ (Quorum K850, United Kingdom) and were subsequently sputter-coated with gold (Safematic CCU-010 HV, Switzerland). Observations were performed using a scanning electron microscope (TESCAN Mira3, Czech Republic), with meticulous recording of the spore chain morphology and spore surface ornamentation of the isolate.

165 rDNA sequencing and phylogenetic analysis: To definitively establish the taxonomic identity of strain HNF214, selected for its potent antibacterial activity, 16S rDNA sequencing and subsequent phylogenetic analyses were performed. Strain HNF214 was cultivated in ISP-2 broth for seven days at 32°C with continuous agitation (150 rpm). Bacterial cells were harvested by centrifugation and thoroughly washed with phosphate-buffered saline (PBS). Genomic DNA was then extracted and the 16S rDNA gene was amplified following the protocol established by

Nakajima *et al.*¹⁹. The specific primers utilized for amplification were 20F (5'-AGTTTGATCCTGGCTC-3') and 1540R (5'-AAGGAG GTGATCCAGCC-3'). Polymerase Chain Reaction (PCR) products were purified using a QIAquick gel extraction kit (Qiagen, Germany), strictly adhering to the manufacturer's guidelines.

Sanger sequencing was conducted by 1st BASE, Singapore. The obtained sequences were compared against reference species in the NCBI BLAST database to determine similarity. Multiple sequence alignment of closely related type strains, retrieved from the GenBank database, was performed using Cluster W. A phylogenetic tree was subsequently constructed using the neighbor-joining method within MEGA 11 software²⁰. *Microbispora corallina* DF-32 (JCM 10267) served as the outgroup for the phylogenetic analysis.

Compound purification and characterization: For the purification of bioactive compounds, 18 g of the crude extract was subjected to silica gel column chromatography (Merck, 0.040-0.063 mm). Elution was performed using a gradient of dichloromethane (CH₂Cl₂) to methanol (MeOH). Fractions containing the target compounds were specifically eluted with 4-5% MeOH in CH₂Cl₂. Subsequent purification steps involved thin-layer chromatography (TLC), employing a CH₂Cl₂:EtOAc (2:5) solvent system. This process successfully yielded 14.86 mg of compound 1 and 17.43 mg of compound 2.

Structural elucidation of the isolated compounds was carried out using a combination of spectroscopic techniques. Melting points were determined with a Stuart SMP20 apparatus (Cole-Parmer). UV spectra were acquired using a Perkin Elmer Lambda 35 spectrophotometer (PerkinElmer). The ¹H-NMR (400MHz) and ¹³C-NMR (100 MHz) spectra were obtained using a Bruker AMX400 NMR spectrometer (Bruker). Finally, molecular weight determination was performed using a POLARIS Q mass spectrometer (Thermo Fisher Scientific).

Determination of minimum inhibitory concentration (MIC) and minimum bactericidal concentration (MBC): The minimum inhibitory concentration (MIC) and minimum bactericidal concentration (MBC) of both the crude extract and the purified compounds were determined to evaluate their antibacterial activity against the relevant bacterial strains. These assays were determined using a standard broth microdilution method²¹. Chloramphenicol (Thermo Fisher Scientific, Massachusetts, USA) served as the positive control.

Determination of cytotoxicity activity: The *in vitro* cytotoxicity of both the crude extract and the purified compounds was assessed using the MTT assay²². Both

samples were tested against three cancer cell lines: Human breast carcinoma cells (MDA-MB-231), human cervical carcinoma (HeLa) and human hepatocellular carcinoma cells (HepG2).

A concentration range from 1 to 512 μ g/mL was used for these assays. To determine the selectivity of the compounds for cancer cells, a non-cancerous cell line, Vero (African green monkey kidney cells), was included in the testing. Selectivity indices (SI) were calculated as the ratio of the IC₅₀ (concentration required for 50% cell growth inhibition) in the Vero cell line to the IC₅₀ in the respective cancer cell lines. A higher SI value indicates that the compound exhibits greater selectivity in targeting cancer cells while minimizing cytotoxicity to healthy cells. For the positive control in the cytotoxicity assay, doxorubicin hydrochloride (Thermo Fisher Scientific, Massachusetts, USA) was utilized.

Molecular docking and ADMET studies: Given that the purified compounds were identified as flavonoids and existing literature suggests that flavonoids can act as potential inhibitors of Mitogen-Activated Protein Kinase (MAPK) proteins, a key cancer therapeutic target²³, further investigation was warranted. This study focused on two specific kinases, MEK1 and MEK2, to understand how their inhibition might contribute to the observed anticancer activity. These protein kinases represent valuable targets due to their unique inhibition binding pocket, which is distinct from the ATP-binding site. This site, characterized by a conserved DFG-out (Asp-Phe-Gly) region (Asp208-Phe209-Gly210 for MEK1; Asp212-Phe213-Gly214 for MEK2)²³, allows inhibitors to bind in an ATP-noncompetitive manner, effectively locking the protein in an inactive state. This mechanism provides higher selectivity compared to other kinase targets²³.

In silico docking studies were performed between these protein kinases and the purified compounds. Three-dimensional models of compounds 1 and 2 were generated using UCSF Chimera, followed by energy minimization to obtain stable conformations. The crystal structures of the protein kinases, MEK1 and MEK2, were retrieved from the Protein Data Bank (PDB IDs: 3DY7 and 1S9I, respectively). Molecular docking simulations were carried out using AutoDock Vina, integrated within the Chimera software package. A grid box of 50x50x50 Å was defined, centered on the DFG-out site of their native inhibitors (1CX; PubChem CID: 46937033 for MEK1 and 5EA; PubChem CID: 5287529 for MEK2), as determined by the co-crystallized ligand in the PDB file. Docking results are reported as binding affinities (kcal/mol), with the lowest energy pose selected for further

analysis. Protein-ligand interactions were visualized and 2D interaction maps were generated using Discovery Studio (BIOVIA). Hydrogen bond and hydrophobic interactions with specific residues were identified using the same software.

Finally, *in silico* ADMET (Absorption, Distribution, Metabolism, Excretion and Toxicity) properties were predicted using the SwissADME, Pre-ADMET and pkCSM online platforms. The ADMET properties of their native inhibitors were used for comparison.

Detection of ERK activation by sandwich ELISA: The MAPK/ERK pathway is crucial for maintaining cellular balance by regulating cell survival and proliferation. Inhibition by the purified compounds is expected to suppress ERK activation. To investigate this, ERK phosphorylation was determined using an ELISA.

The MDA-MB-231 cells (10^4 cells/well) were seeded in 6-well plates and incubated for 24 hrs. The cells were then treated with compounds **1** and **2** at concentrations of $0.5 \times IC_{50}$ and IC_{50} for 24 hrs. Following treatment, cells were lysed using RIPA buffer supplemented with 1% protease/phosphatase inhibitor cocktail. The lysates were then centrifuged at 14,000 rpm for 30 min at 4°C. Phosphorylated tyrosine/threonine in Extracellular-Signal-Regulated Kinase (ERK) 1/2 was quantified using the phospho ERK1/2 (pT202/pY204) sandwich ELISA kit (Invitrogen, Waltham, Massachusetts, USA).

Statistical analysis: All experiments were conducted in triplicate and data are presented as the Mean±Standard Deviation (SD). Statistical significance was assessed using One-way Analysis of Variance (ANOVA), followed by Tukey's *post-hoc* test for multiple comparisons. All statistical analyses were performed using SPSS version 11.01 (SPSS Inc.). A p-value of <0.05 was considered statistically significant.

RESULTS

Five *Apis florea* beehives were sampled, leading to the successful isolation of 32 actinomycete strains. Initial screening for antimicrobial activity via the soft-agar overlay method revealed that one isolate, HNF214, demonstrated significant antibacterial properties. This strain exhibited potent activity against *Bacillus cereus* TISTR687 (Fig. 1a) and *Staphylococcus aureus* TISTR885 (Fig. 1b), producing inhibition zones of 2.8 and 3.6 cm, respectively.

Further characterization of strain HNF214 showed that its spore mass was white (Fig. 2a). Both its aerial and substrate mycelia transitioned from yellow to reddish-brown (Fig. 2b)

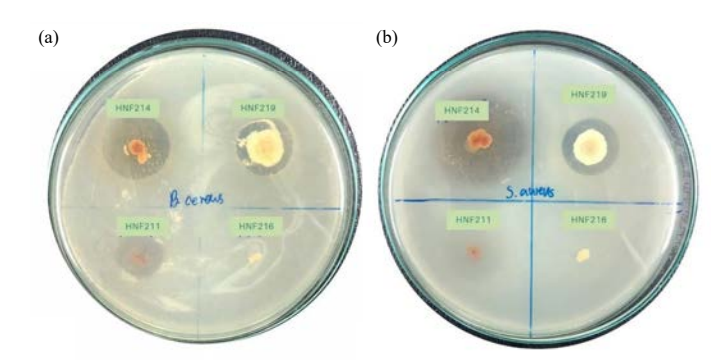


Fig. 1(a-b): Screening of antibacterial activity using the soft-agar overlay technique, panel (a) Inhibition zone formed against *Bacillus cereus* TISTR687 and panel (b) Inhibition against *Staphylococcus aureus* TISTR885, both observed on ISP-2 medium

The antibacterial activity of *Streptomyces griseoaurantiacus* HNF214 against two target bacterial strains using the soft-agar overlay method, for this assay, 7-day-old precultures of *S. griseoaurantiacus* HNF214 were overlaid with soft agar containing the respective test bacterium, following 24 hrs of incubation at 37°C and the diameter of the inhibition zone was measured

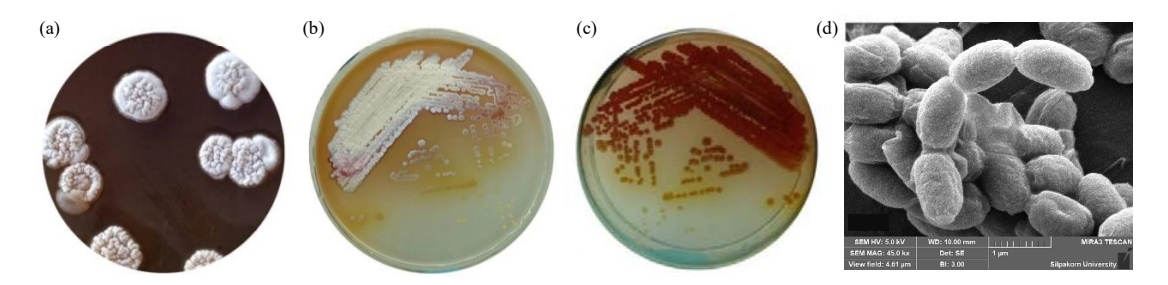


Fig. 2(a-d): Colony characteristics and scanning electron microscope observation of *Streptomyces griseoaurantiacus* HNF214, panel (a) Characteristic white spore mass color, panel (b) Upper side of the colony, revealing aerial and substrate mycelium that transitions from yellow to reddish-brown, panel (c) Production of a yellow diffusible pigment on the reverse side of the ISP-2 agar and panel (d) SEM image showing rectiflexible spore chains with smooth-surfaced, rod-shaped spores

The scale bar in panel (d) represents 1 μ m and the colony characteristics and scanning electron microscope (SEM) observations of *Streptomyces griseoaurantiacus* HNF214 after 21 days of growth on ISP-2 agar at 32°C

and a yellow diffusible pigment was observed on ISP-2 medium (Fig. 2c). Microscopic examination revealed a well-developed, irregularly branched vegetative mycelium without fragmentation of the substrate hyphae. The aerial mycelium displayed monopodial branching and formed flexible chains of arthrosporic with numerous oval to cylindrical spores per chain, each possessing a smooth surface (Fig. 2d). Based on morphological characteristics and the presence of LL-diaminopimelic acid in its cell extract, isolate HNF214 was initially classified as a member of the genus *Streptomyces*.

Bioinformatic analysis of the 16S rRNA gene sequence for strain HNF214 was conducted using the Basic Local Alignment Search Tool (BLAST). The results revealed a high level of similarity to *Streptomyces griseoaurantiacus*, with pairwise sequence comparisons showing 99.80% homology to the 16S rRNA gene sequences of *S. griseoaurantiacus* strain NBRC 15440 (GenBank accession number NR 041186) and strain

AC 38 (GenBank accession number KY412831). This classification was further supported by a phylogenetic analysis (Fig. 3) based on the 16S rRNA gene sequence, which showed HNF214 clustering with the *S. griseoaurantiacus* clade.

The 16S rRNA gene sequence of HNF214 has been deposited in the GenBank database under accession number PV696843.

This study successfully isolated two purified compounds from the crude extract derived from *Streptomyces griseoaurantiacus* HNF214. The chemical structures of these compounds, elucidated through various spectroscopic techniques, are detailed in the subsequent sections.

Compound 1: was a yellow powder; MP 226-227 °C, ESI-MS (positive mode): m/z 303, [M+H]⁺ (Calcd for $C_{15}H_{11}O_7$), m/z 247 [M+H-2CO]⁺; Rv_{max} (KBr) cm⁻¹: 3455, 1690, 1570, 1465, 1080; UV (MeOH) $λ_{max}$ nm: 256 and 357; ¹H-NMR (400 MHz, CD₃OD):

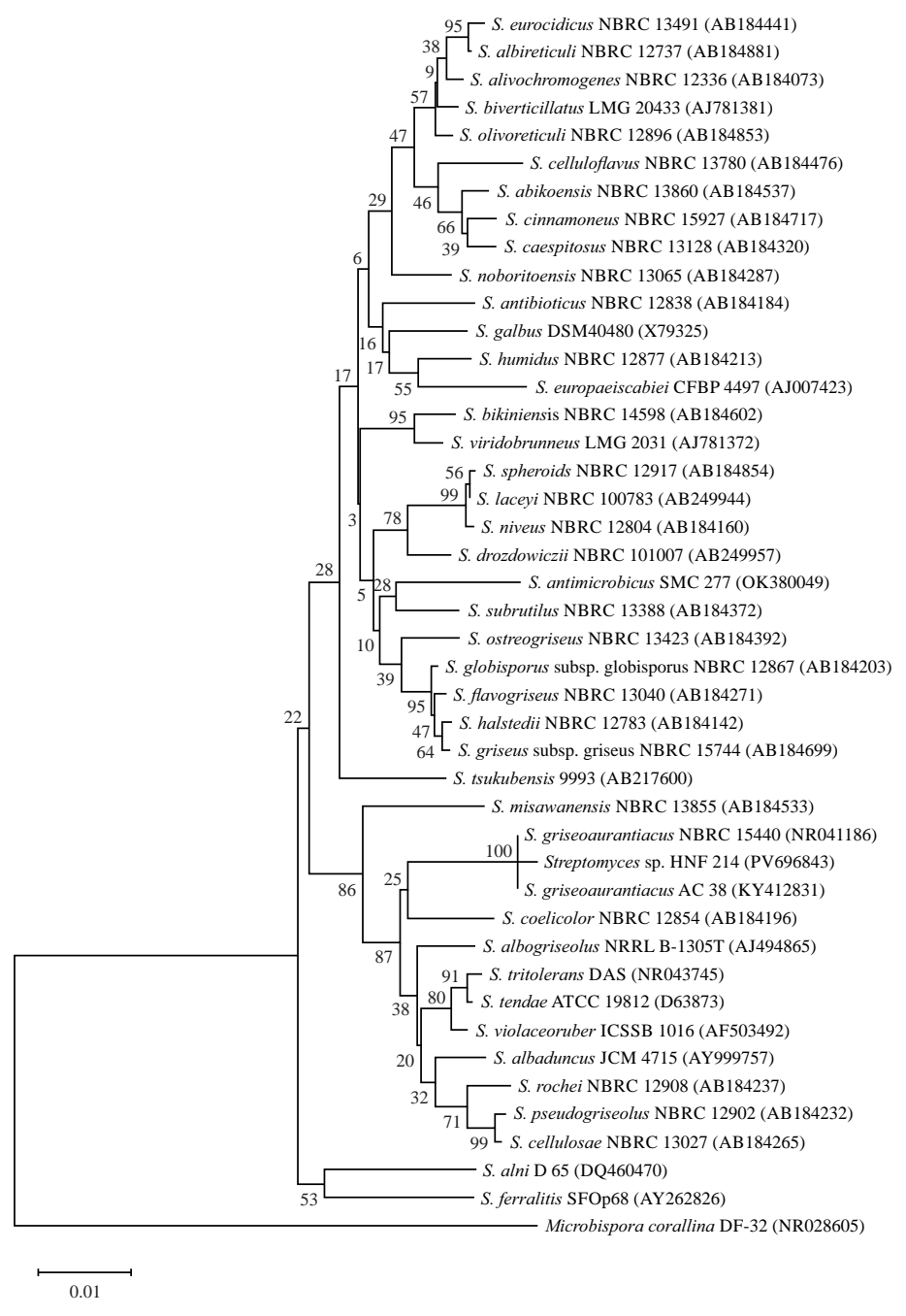


Fig. 3: Phylogenetic analysis of 16S rDNA gene sequences

Phylogenetic analysis of the 16S rDNA gene sequence from *Streptomyces griseoaurantiacus* HNF214 alongside related type strains, whose GenBank accession numbers are provided in parentheses. The phylogenetic tree was constructed using the neighbor-joining method within the MEGA11 software. To assess the robustness of the tree topology, bootstrap analysis was performed with 1000 replicates, and the resulting bootstrap percentages are displayed at each node and the branch length in the figure represents 0.01 substitutions per site

 $δ_H$: 6.21 (1H, brs, H-6), 6.42 (1H, brs, H-8), 6.90 (1H, d, J= 8.5, H-5'), 7.55 (1H, dd, J= 2.2 and 8.5, H-6'), 7.69 (1H, d, J= 2.2, H-2'), 12.50 (1H, s, OH-5); 13 C-NMR (100 MHz, CD $_3$ OD): $δ_C$: 94.2 (C-8), 99.1 (C-6), 103.9 (C-4a), 115.9 (C-2'), 116.5 (C-5'), 120.9 (C-6'), 122.8 (C-1'), 136.6 (C-3), 145.9 (C-3'), 147.7 (C-4'), 148.5 (C-2), 156.9 (C-8a), 161.6 (C-5), 164.7 (C-7), 176.7 (C-4).

Compound 2: was a yellow powder; MP 232-233 °C, ESI-MS (positive mode): m/z 465, [M+H]⁺ (Calcd for C₂₁H₂₀O₁₂), m/z 303 [M+H-Glc]⁺; IRυ_{max} (KBr) cm⁻¹: 3450, 1688, 1560, 1460, 1075; UV (MeOH)λ_{max} nm: 257 and 358; ¹H-NMR (400 MHz, CD₃OD): δ_H: 5.25 (1H, d, J= 7.5, H-1"), 6.23 (1H, d, J= 2.1, H-6), 6.42 (1H, d, J= 2.1, H-8), 6.91 (1H, d, J= 8.5, H-5"), 7.61 (1H, dd, J= 2.2 and

Fig. 4(a-b): Structures of the compounds, (a) Quercetin and (b) Quercetin-3-O-β-D-glucopyranoside (isoquercetin)

Table 1: MIC of the purified compounds and crude extract against tested bacteria

		MIC (mg/mL)						
Test substances	S.a.	S.e.	B.c.	B.s.	MRSA Sp3	E.c.	S.t.	P.a.
Crude extract	512	512	512	512	512	512	512	512
Compound 1	256	256	256	256	256	>512	>512	>512
Compound 2	256	256	256	256	256	>512	>512	>512
Chloramphenicol	2	2	2	2	8	16	16	32

S.a.: Staphylococcus aureus TISTR885, S.e.: Staphylococcus epidermidis TISTR518, B.c.: Bacillus cereus TISTR687, B.s.: Bacillus subtilis TISTR008, MRSA Sp3: Methicillin-resistant Staphylococcus aureus Sp3, E.c.: Escherichia coli TISTR887, S.t.: Salmonella typhimurium TISTR292 and P.a.: Pseudomonas aeruginosa TISTR1287

Table 2: MBC of the purified compounds and crude extract against tested bacteria

Test substances	MBC (mg/mL)							
	S.a.	S.e.	B.c.	B.s.	MRSA Sp3	E.c.	S.t.	P.a.
Crude extract	>512	>512	>512	>512	>512	>512	>512	>512
Compound 1	>512	>512	>512	>512	>512	>512	>512	>512
Compound 2	>512	>512	>512	>512	>512	>512	>512	>512
Chloramphenicol	16	16	16	16	32	32	32	64

S.a.: Staphylococcus aureus TISTR885, S.e.: Staphylococcus epidermidis TISTR518, B.c.: Bacillus cereus TISTR687, B.s.: Bacillus subtilis TISTR008, MRSA Sp3: Methicillinresistant Staphylococcus aureus Sp3, E.c.: Escherichia coli TISTR887, S.t.: Salmonella typhimurium TISTR292 and P.a.: Pseudomonas aeruginosa TISTR1287

8.5, H-6'), 7.73 (1H, d, J= 2.2, H-2'); 13 C-NMR (100 MHz, CD $_3$ OD): δ_C : 60.9 (C-6"), 70.2 (C-4"), 74.7 (C-2"), 77.1 (C-5"), 77.4 (C-3"), 93.9 (C-8), 98.8 (C-6), 103.3 (C-1"), 104.6 (C-4a), 115.2 (C-2'), 116.6 (C-5'), 121.9 (C-1'), 122.1 (C-6'), 134.6 (C-3), 144.9 (C-3'), 148.9 (C-4'), 157.5 (C-2), 158.1 (C-8a), 161.9 (C-5), 165.1 (C-7), 178.6 (C-4).

Structural elucidation of the purified compounds revealed their identities as quercetin (compound 1) (Fig. 4a) and quercetin-3-O-β-D-glucopyranoside (isoquercetin) (compound 2) (Fig. 4b), respectively. During the isolation process, it was determined that *Streptomyces griseoaurantiacus* HNF214 produced quercetin at a concentration of 0.83 mg/g of crude extract (or 0.99 mg/L of culture medium) and isoquercetin at 0.97 mg/g of crude extract (or 1.16 mg/L of culture medium).

Using a microbroth dilution assay, researchers evaluated the antimicrobial activity of both the crude extract and the purified compounds by measuring their minimum inhibitory concentrations (MICs) and minimum bactericidal concentrations (MBCs). The purified compounds displayed

selective antibacterial effects, primarily acting against Grampositive bacteria.

Specifically, these compounds inhibited the growth of several strains, including <code>Staphylococcus aureus</code> TISTR885, <code>Staphylococcus epidermidis TISTR518</code>, <code>Bacillus cereus TISTR687</code>, <code>Bacillus subtilis TISTR008</code> and the clinical isolate methicillin-resistant <code>S. aureus Sp3</code>. For these strains, the MIC was determined to be 256 µg/mL, while the MBC values were found to be greater than 512 µg/mL, as detailed in Table 1 and 2.

The cytotoxic effects of the crude extract and its purified components were evaluated against Vero (non-cancerous), MDA-MB-231 (breast carcinoma), HeLa (cervical carcinoma) and HepG2 (hepatocellular carcinoma) cell lines. The crude extract generally showed lower cytotoxicity compared to the purified compounds.

The purified compounds demonstrated significant cytotoxicity against several cancer cell lines, though not against the non-cancerous Vero cells. The IC_{50} values for the compounds against MDA-MB-231 and HeLa cells were

Table 3: IC_{so} values and selectivity indices (SI) of crude extract and purified compounds against cancer cell lines

	Vero cells*	MDA-MB-231 cells		HeLa cells		HepG2 cells	
Test substances	IC ₅₀ (mg/mL)**	IC ₅₀ (mg/mL)	SI**	IC ₅₀ (mg/mL)	SI	IC ₅₀ (mg/mL)	SI
Crude extract	1262.73±104.37ª	567.04±62.33ª	2.23	628.39±85.67ª	2.01	1163.74±230.28ª	1.09
Compound 1	754.38±72.86 ^b	234.12±35.81 ^b	3.22	398.15±69.93b	1.89	732.18±104.52 ^b	1.03
Compound 2	835.94±98.67b	312.07±48.57b	2.68	487.38±94.11 ^b	1.72	810.62±116.47b	1.03
Doxorubicin hydrochloride	142.67±34.78°	12.05±7.26 ^c	11.84	19.25±9.71°	7.41	135.41±49.88 ^c	1.05

*Vero cells: African green monkey kidney cell line, MDA-MB-231 cells: Human breast cancer cell line, HeLa cells: Human cervical carcinoma cell line, HepG2: Human hepatocellular carcinoma cell line, **IC₅₀ values represent the concentration causing 50% growth inhibition. The values are expressed as Mean \pm Standard Deviation of the three replicates, **SI: Selectivity indices (SI) were calculated as the ratio of the IC₅₀ in the Vero cell line to the IC₅₀ in the cancer cell lines and ^{abc}Different letters indicated statistically significant differences within the same category (p<0.05)

between 234.12 and 312.07 μ g/mL and 398.15 and 487.38 μ g/mL, respectively. The HepG2 cells were less sensitive, with IC₅₀ values ranging from 732.18 to 810.62 μ g/mL. In contrast, neither the crude extract nor the purified compounds were cytotoxic to Vero cells, as their IC₅₀ values exceeded 700 μ g/mL.

The MDA-MB-231 cells showed the highest sensitivity to the purified compounds, comparable to the positive control, doxorubicin hydrochloride. While HeLa and HepG2 cells were affected, their sensitivity was lower than that of MDA-MB-231 cells. Among the tested substances, compound 1 was the most potent after 24 hrs, with IC50 values of 234.12 \pm 35.81 µg/mL against MDA-MB-231 and 398.15 \pm 69.93 µg/mL against HeLa cells. Importantly, the IC50 values for the cancer cell lines were substantially lower than those for the non-cancerous Vero cells.

As shown in Table 3, the selectivity indices (SI) for the crude extract and purified compounds were generally lower than doxorubicin hydrochloride, indicating a comparatively reduced overall selectivity. However, the heightened susceptibility observed in MDA-MB-231 cells suggests a potentially enhanced selectivity toward this particular cell line.

Molecular docking simulations were conducted to elucidate the putative anticancer mechanisms of compounds 1 and 2 by investigating their interactions with key protein kinases. Small molecule inhibitors (native inhibitors) known to target these proteins served as comparative references. The investigation focused on determining the optimal binding poses and associated energies within the DFG-out (Asp-Phe-Gly) pocket site of each protein.

The calculated relative binding energies for compound 1 with MEK1 and MEK2 were -6.71 and -7.57 kcal/mol, respectively. For compound 2, the calculated relative binding energies with MEK1 and MEK2 were -8.99 and -9.09 kcal/mol, respectively. These favorable energies indicate a strong interaction of both compounds within the DFG-out pocket

site, primarily attributed to hydrogen bonding. Detailed specifications regarding hydrogen bond donors, acceptors, interacting residues and bond lengths for MEK1 and MEK2 are presented in Table 4 and 5, respectively.

Analysis of molecular docking simulations revealed key hydrogen bond interactions within the DFG-out (Asp-Phe-Gly) site of MEK1 and MEK2. For MEK1, a critical hydrogen bond was observed between Asp208 and compounds 1, 2, as well as the native inhibitor, as depicted in Fig. 5(a-f), respectively. Additional hydrogen bonds and other interactions were also identified within this pocket.

Similarly, for MEK2, a crucial hydrogen bond interaction involved Asp212 with compound **1** and the native inhibitor (Fig. 6a-f). Notably, an electrostatic (Pi-anion) interaction was observed between Asp212 and compound **2** (Fig. 6c-d). Other hydrogen bonds and interactions were also present in this binding pocket. Furthermore, hydrophobic interactions between the compounds and various residues within the DFG-out pocket of both MEK1 and MEK2 proteins contributed to the overall stability of the formed complexes.

In silico ADMET (Absorption, Distribution, Metabolism, Excretion and Toxicity) prediction was performed to evaluate the pharmacokinetic and toxicological profiles of the compounds. This analysis utilized well-established online platforms, including SwissADME, PreADMET and pkCSM, which are valuable resources for virtual screening in modern drug discovery. These predictive tools offer insights into absorption, distribution, metabolism, excretion and toxicity, thereby facilitating the selection of optimal candidates that meet specific criteria for advancement in new drug development initiatives. The comprehensive results are presented in Table 6.

The inhibitory effects of compounds **1** and **2** on ERK1/2 activation were assessed using a sandwich ELISA to further confirm their involvement with the MAPK/ERK pathway. As illustrated in Fig. 7, both compounds significantly reduced the phosphorylation of ERK1/2 in a dose-dependent manner. At a concentration of 0.5x IC₅₀, compound **1** resulted in

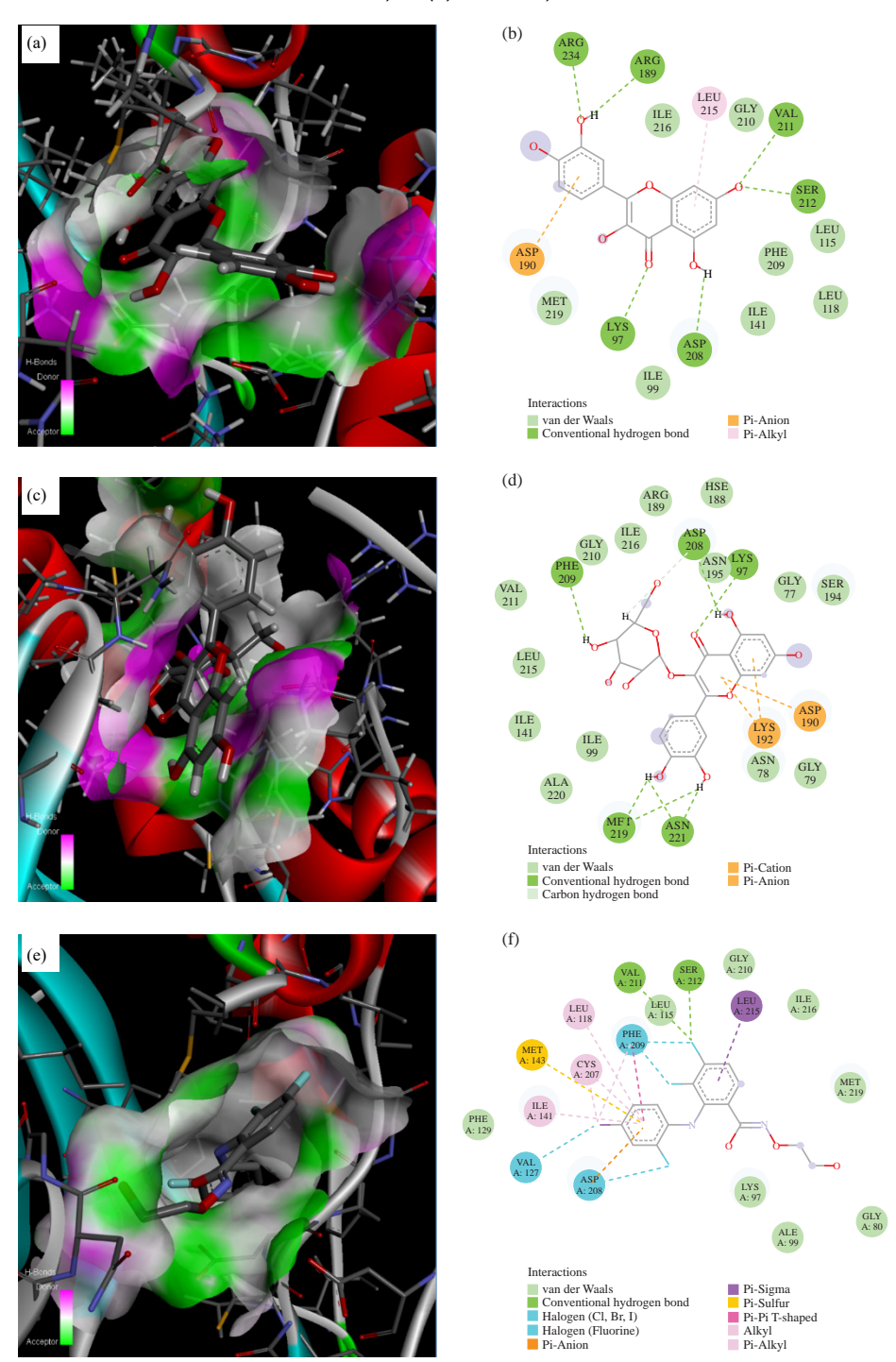


Fig. 5(a-f): Crystal structure interaction and 2D illustration of ligands within the MEK1 DFG-out Site (PDB ID: 3DY7). Interaction of compound **1** with MEK1, (a) Crystal structure view, (b) 2D interaction diagram. Interaction of compound **2** with MEK1, (c) Crystal structure view, (d) 2D interaction diagram. Interaction of the native inhibitor (1CX) with MEK1, (e) Crystal structure view and (f) 2D interaction diagram

Figure presents the binding modes of compound 1, compound 2 and the native inhibitor (1CX) within the DFG-out (Asp-Phe-Gly) site of MEK1, (This original figure was generated using Discovery Studio (BIOVIA) software after molecular docking simulations performed with AutoDock Vina and visualization in Chimera), within the binding cavity, hydrogen bond donors are represented in pink and acceptors in green. The various dashed lines indicate different types of interactions: Dark green for conventional hydrogen bonds, light green for carbon-hydrogen bonds, deep pink for pi-pi stacked, pale pink for alkyl, short pale pink for pi-alkyl, deep brown for pi-cation, light brown for pi-anion, pale brown for pi-sulfur, light blue for halogen and light purple for pi-sigma interactions and amino acids shown in pale green exhibit Van der Waals interactions

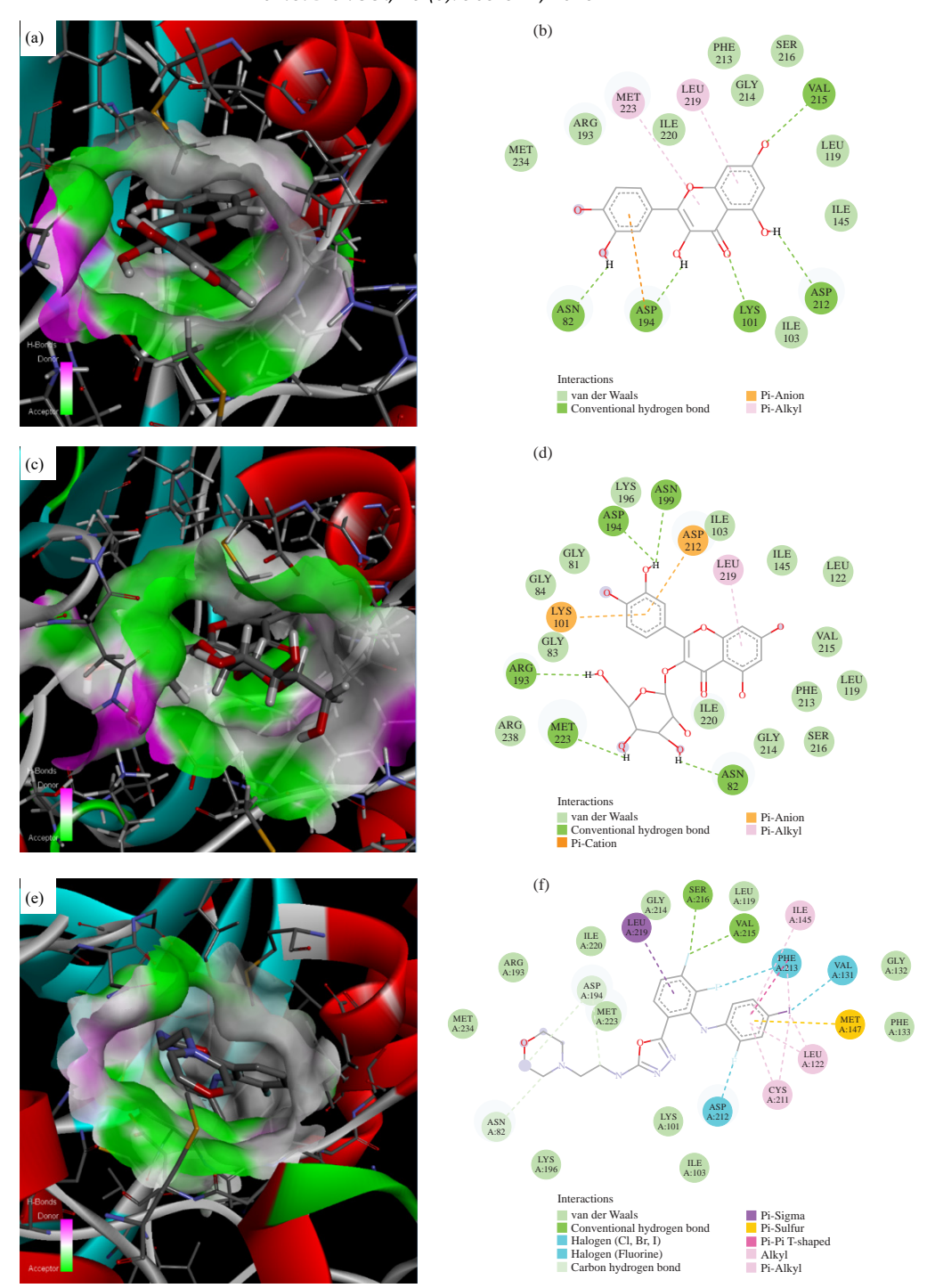


Fig. 6(a-f): Crystal structure interaction and 2D illustration of ligands within the MEK2 DFG-out Site (PDB ID: 1S9I). Interaction of compound 1 with MEK2: (a) Crystal structure view, (b) 2D interaction diagram. Interaction of compound 2 with MEK2, (c) Crystal structure view, (d) 2D interaction diagram. Interaction of the native inhibitor (5EA) with MEK2, (e) Crystal structure view and (f) 2D interaction diagram

Figure presents the binding modes of compound 1, compound 2 and the native inhibitor (5EA) within the DFG-out (Asp-Phe-Gly) site of MEK2, (This original figure was generated using Discovery Studio (BIOVIA) software after molecular docking simulations performed with AutoDock Vina and visualization in Chimera), within the binding cavity, hydrogen bond donors are represented in pink and acceptors in green. The various dashed lines indicate different types of interactions: Dark green for conventional hydrogen bonds, light green for carbon-hydrogen bonds, deep pink for pi-pi t-shaped, pale pink for alkyl, short pale pink for pi-alkyl, deep brown for pi-cation, light brown for pi-anion, pale brown for pi-sulfur, light blue for halogen, and light purple for pi-sigma interactions and amino acids shown in pale green exhibit Van der Waals interactions

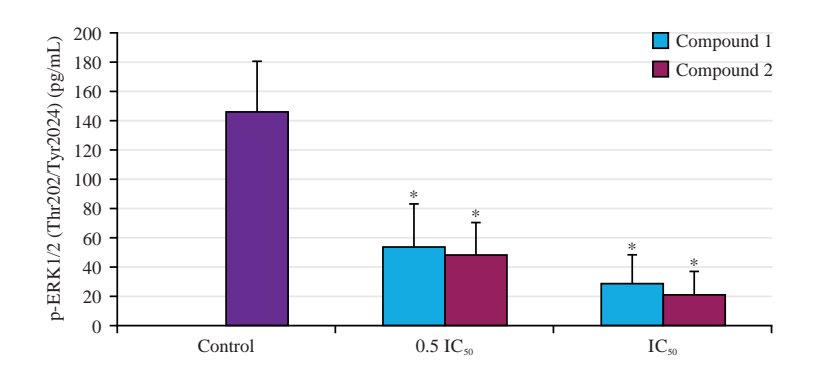


Fig. 7: Quantitative determination of phosphorylated ERK

Quantitative determination of phosphorylated ERK in cell lysates, detected by sandwich ELISA, following 24 hrs treatment with various concentrations of compounds 1 and 2. The data presented represent the Mean±Standard Deviation of three independent experiments and statistical significance of the differences compared with the control (untreated cells) is denoted by *p<0.05

Table 4: Results of predictions of molecular interaction between various MEK1* and the purified compounds

			Hydrogen bo	onds			
Purified compounds	Binding energy (kcal/mol)	Interaction types**	H-bond donors	H-bond acceptors	Bond length (A°)	Docking site	
Compound 1	-6.70604	СоН	LYS97: HZ2	LIG***: O3	2.69257	DFG-out pocket site	
		CoH	VAL211: HN	LIG: O1	2.65977		
		CoH	SER212: HN	LIG: O1	2.26180		
		CoH	ARG234: HH22	LIG: 06	2.22539		
		CoH	LIG: H3	ASP208: OD2	2.93708		
		CoH	LIG: H7	ARG189: O	2.53920		
		Pi-An	ASP190: OD2 (Negative)	LIG (Pi-orbitals)	3.99814		
		Pi-A	LIG (Pi-orbitals)	LEU215 (Alkyl)	4.75306		
Compound 2	-8.99349	СоН	LYS97: HZ2	LIG: O1	2.50813	DFG-out pocket site	
		CoH	LIG: H12	ASP208: OD1	2.37547		
		CoH	LIG: H16	PHE209: O	2.76006		
		CoH	LIG: H19	MET219: O	2.90252		
		CoH	LIG: H19	ASN221: OT2	1.68775		
		CoH	LIG: H20	MET219: O	2.74770		
		CoH	LIG: H20	ASN221: OT2	1.91906		
		CaH	LIG: H5	ASP208: O	2.70733		
		Pi-Ca	LYS192: NZ (Positive)	LIG (Pi-orbitals)	3.87541		
		Pi-Ca	LYS192: HZ3 (Positive)	LIG (Pi-orbitals)	2.78683		
		Pi-An	ASP190: OD2 (Negative)	LIG (Pi-orbitals)	3.84753		
1CX	-9.92440	СоН	VAL211: N	LIG: F1	3.24146	DFG-out pocket site	
		CoH	SER212: N	LIG: F1	3.23648		
		Ha	VAL127: O	LIG: I1	3.35420		
		Ha	ASP208: OD2	LIG: F3	3.18117		
		Ha	PHE209: O	LIG: F1	3.38724		
		Ha	PHE209: O	LIG: F2	3.63530		
		Pi-An	ASP208: OD2 (Negative)	LIG (Pi-orbitals)	3.97414		
		Pi-Si	LEU215: CD2	LIG (Pi-orbitals)	3.90923		
		Pi-Su	MET143: SD	LIG (Pi-orbitals)	5.23323		
		Pi-Pi T	PHE209 (Pi-orbitals)	LIG (Pi-orbitals)	5.25810		
		Α	LIG: I1 (Alkyl)	CYS207 (Alkyl)	5.23279		
		Pi-A	PHE209 (Pi-orbitals)	LIG: I1 (Alkyl)	4.95406		
		Pi-A	LIG (Pi-orbitals)	LEU118 (Alkyl)	5.25532		
		Pi-A	LIG (Pi-orbitals)	ILE141 (Alkyl)	4.95701		
		Pi-A	LIG (Pi-orbitals)	CYS207 (Alkyl)	5.42477		

^{*}MEK1; PDB ID: 3DY7. **Interaction types, CoH: Conventional hydrogen bond, CaH: Carbon hydrogen bond, Ha: Halogen interaction, A: Alkyl interaction, Pi-A: Pi-Alkyl interaction, Pi-An: Pi-Anion interaction, Pi-Ca: Pi-Cation interaction, Pi-Si; Pi-Sigma interaction, Pi-Su; Pi-Sulfur interaction, Pi-Pi T; Pi-Pi T shaped. ***LIG; Ligand: Compounds 1, 2 and native inhibitor (1CX; PubChem CID: 46937033)

Table 5: Results of predictions of molecular interaction between various MEK2* and the purified compounds

·			Hydrogen bo	onds			
Purified compounds	Binding energy (kcal/mol)	Interaction types**	H-bond donors	H-bond acceptors	Bond length (A°)	Docking site	
Compound 1	-7.57401	СоН	LYS101: HZ2	LIG***: O3	2.25175	DFG-out pocket site	
		CoH	VAL215: HN	LIG: O1	2.73102		
		CoH	LIG: H3	ASP212: OD1	3.03507		
		CoH	LIG: H5	ASP194: OD2	2.37141		
		CoH	LIG: H7	ASN82: OD1	2.17896		
		Pi-An	ASP194: OD2 (Negative)	LIG (Pi-orbitals)	4.04106		
		Pi-A	LIG (Pi-orbitals)	LEU219 (Alkyl)	4.82493		
		Pi-A	LIG (Pi-orbitals)	MET223 (Alkyl)	5.46257		
Compound 2	-9.09246	CoH	LIG: H15	ARG193: O	2.86380	DFG-out pocket site	
		СоН	LIG: H16	MET223: OT2	2.35357		
		CoH	LIG: H17	ASN82: OD1	1.97851		
		СоН	LIG: H19	ASP194: OD2	2.12416		
		CoH	LIG: H19	ASN199: OD1	2.48481		
		Pi-Ca	LYS101: NZ (Positive)	LIG (Pi-orbitals)	3.46464		
		Pi-An	ASP212: OD2 (Negative)	LIG (Pi-orbitals)	3.46990		
		Pi-A	LIG (Pi-orbitals)	LEU219 (Alkyl)	4.90705		
5EA	-12.20142	СоН	VAL215: N	LIG: F17	2.89175	DFG-out pocket site	
		CoH	SER216: N	LIG: F17	2.63074		
		CaH	LIG: C22	ASP194: OD2	3.49317		
		CaH	LIG: C27	ASN82: OD1	3.13127		
		CaH	LIG: C29	ASP194: OD1	3.42876		
		Ha	VAL131: O	LIG: I1	3.24970		
		Ha	ASP212: OD1	LIG: F20	3.23934		
		Ha	PHE213: O	LIG: F1	3.53004		
		Pi-Si	LEU219: CD1	LIG (Pi-orbitals)	3.98817		
		Pi-Su	MET147: SD	LIG (Pi-orbitals)	5.29234		
		Pi-Pi T	PHE213 (Pi-orbitals)	LIG (Pi-orbitals)	4.91449		
		Α	LIG: I1 (Alkyl)	LEU122 (Alkyl)	4.84609		
		Α	LIG: I1 (Alkyl)	CYS211 (Alkyl)	5.04472		
		Pi-A	PHE213 (Pi-orbitals)	LIG: I1 (Alkyl)	4.68043		
		Pi-A	LIG (Pi-orbitals)	LEU122 (Alkyl)	5.30497		
		Pi-A	LIG (Pi-orbitals)	ILE145 (Alkyl)	5.00525		
		Pi-A	LIG (Pi-orbitals)	CYS211 (Alkyl)	5.16931		

*MEK2; PDB ID: 1S9I. **Interaction types, CoH: Conventional hydrogen bond, CaH: Carbon hydrogen bond, Ha: Halogen interaction, SB: Salt bridge, A: Alkyl interaction, Pi-A: Pi-Alkyl interaction, Pi-An: Pi-Anion interaction, Pi-Ca: Pi-Cation interaction, Pi-Si; Pi-Sigma interaction, Pi-Su; Pi-Sulfur interaction, Pi-Pi T; Pi-Pi T shaped. ***LIG; Ligand: Compounds 1, 2 and native inhibitor (5EA; PubChem CID: 5287529)

53.56 pg/mL and compound **2** in 48.41 pg/mL of phosphorylated ERK1/2. When the concentration was increased to IC_{50} , the levels further decreased to 28.75 pg/mL for compound **1** and 21.23 pg/mL for compound **2**. These findings indicate that treatment with compounds **1** and **2** inhibits the MAPK/ERK pathway by suppressing ERK1/2 phosphorylation.

DISCUSSION

This investigation successfully isolated and identified two known bioactive flavonoids, quercetin (compound 1) and isoquercetin (compound 2), from *Streptomyces griseoaurantiacus* HNF214. Their identities were confirmed through comparative analysis of the purified compounds' spectral data with previously published literature. For instance, the spectral characteristics of our isolated quercetin showed

notable similarities to those reported by Gopikrishnan *et al.*²⁴ for quercetin obtained from the marine-derived actinobacterium *Streptomyces fradiae* PE7, thus supporting our identification.

Quercetin derivatives are widely distributed in various plant species, including numerous fruits and vegetables^{25,26}. Well-known dietary sources of quercetin include *Malus domestica* (apple), *Pyrus communis* (pear), *Solanum lycopersicum* (tomato), *Ipomoea batatas* (sweet potato), *Sambucus canadensis* (elderberry), *Fragaria ananassa* (strawberry), *Capsicum annuum* (bell pepper), *Carica papaya* (papaya), *Lactuca capitata* (lettuce), *Phaseolus vulgaris* (common bean), *Vitis vinifera* (grape), *Prunus dulcis* (almond), *Pistacia vera* (pistachio), *Juglans regia* (walnut) and *Coffea arabica* (coffee)^{27,28}. Beyond plants, quercetin has also been reported from actinobacteria such as *Streptomyces fradiae* PE7²⁴ and *Streptomyces antibioticus* strain ess_amA8²⁹.

Table 6: Predicted absorption, distribution, metabolism, excretion and toxicity properties of the compound agents

	Compound agents						
Properties	Compound 1		Doxorubicin				
TPSA	131.36	210.51	206.07				
Consensus log P _{o/w}	1.23	-0.25	0.50				
Absorption							
Water solubility (log S)	-3.24	-1.51	-5.20				
Caco2 cell permeability	3.41	9.44	17.72				
Human intestinal absorption (% absorbed)	75.09	40.51	31.95				
Skin permeability (log Kp cm/s)	-2.74	-2.74	-4.69				
P-Glycoprotein substrate	No	No	No				
P-Glycoprotein inhibitor	No	No	No				
Distribution							
BBB permeability (log BBB)	-1.3750	0.0320	0.0328				
Metabolism							
CYP2D6 substrate	No	No	Weakly				
CYP3A4 substrate	No	No	Weakly				
CYP1A2 inhibitor	Yes	No	No				
CYP2C19 inhibitor	No	No	No				
CYP2C9 inhibitor	No	No	No				
CYP2D6 inhibitor	No	No	No				
CYP3A4 inhibitor	No	No	No				
Excretion							
Renal OCT2 substrate	No	No	No				
Toxicity							
Ames_test	Mutagen	Non-mutagen	Mutagen				
Carcino_mouse	No	No	No				
Carcino_rat	Yes	No	No				
TA100_10RLI	No	No	No				
TA100_NA	Yes	No	No				
TA1535_10RLI	No	No	No				
TA1535_NA	No	No	No				
hERG inhibitor	No	No	Ambiguous				
Hepatotoxicity	No	No	Yes				
Skin sensitization	No	No	No				

BBB: Blood-brain barrier, CYP: Cytochrome p450, Caco2: Caucasian colon adenocarcinoma cell line, hERG: Human ether-a-go-go-related gene, Kp: Skin permeability constant, log $P_{o/w}$: log of relative solubility of the drug in n-octanol, OCT2: Organic cation transporter 2 and TPSA: Topological polar surface area

This investigation involved two main parts: first, the isolation and taxonomic identification of the producing organism, *Streptomyces griseoaurantiacus* HNF214. The second part focused on the purification of its quercetin metabolites and their subsequent biological evaluation for antibacterial and anticancer properties. It's important to note that quercetin yields can vary considerably among *Streptomyces* species and under different culture conditions. For example, *Streptomyces fradiae* PE7, isolated from Velar estuarine sediment in South India, was reported to produce quercetin at 100 mg/g of crude extract (10%)²⁴. Our study, in contrast, documented the isolation of *Streptomyces griseoaurantiacus* HNF214 from an *Apis florea* beehive, showing a noteworthy quercetin yield of 0.83 mg/g and an isoquercetin yield of 0.97 mg/g of crude extract.

Phylogenetic analysis confirmed a close evolutionary relationship between HNF214 and *S. griseoaurantiacus* strain NBRC 15440 and strain AC 38. *S. griseoaurantiacus* has been

previously isolated from various environments, including leaf litter in the semiarid region of Aiuaba, Ceará State, Brazil³⁰ and soil samples in India³¹. Past research has reported this species to have antagonistic effects on rhizobia³⁰ and to possess anticancer properties³¹. Specifically, *S. griseoaurantiacus* JUACT01, isolated from Indian soil samples, produced a yellow pigment that exhibited cytotoxicity against HeLa cells and HepG2 cells, with IC₅₀ values of 1.5 and 1.8 μ g/mL, respectively. This pigment was also reported to have non-toxic effects on human lymphocytes³¹.

Quercetin and its derivatives are well-documented for their antibacterial properties. In this study, the isolated quercetin and isoquercetin exhibited antibacterial activity exclusively against Gram-positive bacteria. This selective activity might be attributed to their ability to permeate the distinct cell wall and cell membrane structures of these organisms. Literature suggests that quercetin employs several mechanisms to exert its antimicrobial effects. It can disrupt

bacterial cell envelope synthesis by targeting fatty acid synthase (FAS) and interfering with peptidoglycan formation. Furthermore, quercetin is known to directly destabilize bacterial cell membranes and impede nucleic acid synthesis through DNA gyrase inhibition. Beyond these direct actions, quercetin can also mitigate bacterial virulence factors, including toxins. Its flavonoid structure enables it to inhibit efflux pumps, potentially reversing antimicrobial resistance and it can also suppress ATP synthase. These diverse modes of action highlight quercetin's promise as an antimicrobial agent ^{32,33}.

Beyond its antimicrobial potential, quercetin is also recognized as a promising anticancer agent, with applications as a complementary or alternative medication for cancer prevention and treatment³⁴. In the current study, the isolated quercetin and isoquercetin demonstrated cytotoxic activity against MDA-MB-231 (breast), HeLa (cervical) and HepG2 (liver) cancer cell lines, with IC50 values ranging from 234.12 to 810.62 µg/mL. These results indicate a significant impact on cancer cell viability. However, the observed cytotoxicity against non-cancerous Vero cells (IC₅₀: 754.38 to 835.94 µg/mL) underscores the necessity for optimizing these compounds to enhance their selectivity. While the compounds showed relatively lower cytotoxicity towards Vero cells compared to cancer cells, minimizing toxicity to normal cells remains crucial for therapeutic development. Interestingly, guercetin and isoguercetin exhibited a similar selectivity index (SI) against HepG2 cells when compared to doxorubicin hydrochloride, suggesting their potential as alternative treatments for hepatocellular carcinoma.

Flavonoids are known to influence cancer progression by inhibiting proliferation, angiogenesis and metastasis, or by inducing apoptosis, autophagy and cell cycle arrest. These effects are often achieved through interference with various signal transduction pathways³⁵⁻³⁷. Within cellular signaling, certain flavonoids can bind to and alter the phosphorylation of protein kinases, such as MAP kinases. The deregulation of the MAPK cascade is a hallmark of uncontrolled cancer cell proliferation and survival, making it a crucial therapeutic target for various cancer conditions.

The MEK1 and MEK2 are dual-specificity kinases that are directly phosphorylated and activated to subsequently activate ERK1 and ERK2 via phosphorylation. As the sole activators of ERK1/2, MEK1 and MEK2 are highly significant, as ERK1/2 in turn targets numerous proteins controlling cancer cell survival, differentiation and progression. These enzymes are considered valuable therapeutic targets due to their unique inhibition binding pocket. This pocket, distinct from the ATP-binding site and characterized by a conserved

DFG-out (Asp-Phe-Gly) region, allows inhibitors to bind in an ATP-noncompetitive manner. This mechanism effectively locks the protein in an inactive state, conferring higher selectivity compared to other kinase targets. Given their roles in tumorigenesis, MEK1 and MEK2 represent excellent therapeutic targets for controlling cancer cell survival, differentiation and progression. Notably, quercetin has previously been reported to bind to MEK1 and inhibit its kinase activity without competing with ATP at the DFG-out pocket site.

To investigate quercetin and isoquercetin as potential inhibitors targeting MEK1 and MEK2 for downregulation of the MAPK pathway, molecular docking simulations were performed with quercetin, isoquercetin and their native inhibitors (1CX for MEK1/PDB ID: 3DY7 and 5EA for MEK2/PDB ID: 1S9I). These compounds were found to interact within the DFG-out pocket site, sharing a common key residue: Asp208 on MEK1 or Asp212 on MEK2. Consistent with previous reports, flavonoids, including those in this study, demonstrate high docking affinity for MEK2, with Asp212 consistently identified as a crucial interaction residue contributing to the binding energy²³. The shared amino acid interactions between compounds 1 and 2 and the native inhibitors suggest a potentially similar mechanism of protein inhibition.

The binding energies obtained from the docking studies revealed favorable interactions between the compounds and the target proteins. Although compounds 1 and 2 showed slightly higher binding energies (less negative) than the native inhibitors, which benefit from additional halogen interactions, compounds 1 and 2 displayed a greater number of conventional hydrogen bond interactions. This suggests enhanced stability of their interactions, potentially leading to a more stable binding compared to the native inhibitors of MEK1 and MEK2. Significantly, the binding energy of compound 2 to both MEK1 and MEK2 was lower (more favorable) than that of compound 1. This suggests that the presence of the additional glycoside group in compound 2 enhances its interaction stability with amino acid residues, aligning with reports of flavonoid glycosides exhibiting lower binding energies in interactions with HIV-1 reverse transcriptase³⁸ and SARS-CoV-2 protease and RNA-dependent RNA polymerase³⁹.

Since MEK1 and MEK2 are dual-specificity kinases that directly phosphorylate and activate ERK1 and ERK2, our finding that treatments with compounds 1 and 2 significantly decreased p-ERK1/2 levels in the sandwich ELISA is highly relevant. This result suggests that these compounds can inactivate MEK1 and MEK2, leading to MAPK pathway inhibition and subsequently controlling cancer cell

proliferation and survival. Previous studies have reported that quercetin can block the MAPK/ERK pathway by inhibiting ERK phosphorylation, which is essential for its activation and subsequent nuclear translocation. Once in the nucleus, activated ERK promotes the expression of genes involved in cell division and survival⁴⁰. By reducing ERK activation, quercetin decreases the transcription of these oncogenic targets, leading to reduced cellular proliferation and increased apoptosis in cancer cells. For instance, studies in lung cancer cell lines indicate that quercetin treatment effectively reduces ERK phosphorylation, impairing cell cycle progression and promoting apoptotic cell death. Furthermore, the inhibition of the MAPK/ERK pathway by quercetin can enhance the efficacy of other anticancer treatments⁴¹.

In silico ADMET predictions, performed using the SwissADME, PreADMET and pkCSM platforms, provided insights into the pharmacokinetic and toxicological profiles of the isolated compounds. The results indicated moderate human intestinal absorption for both compounds, with values ranging from 30 to 70% (values below 30% are considered poorly absorbed)⁴²⁻⁴⁴. Specifically, compound 1 was predicted to be well absorbed, while compound 2 showed moderate absorption.

To further evaluate intestinal permeability, predictions for Caco-2 cell line permeability (representing the human intestinal epithelium) were generated. Both compounds were found to have favorable pharmacokinetic properties. They demonstrated high Caco-2 permeability, with predicted values exceeding 0.90, which indicates good oral absorption. For applications like transdermal drug delivery and dermal toxicity assessment, skin permeability is also a crucial factor; in this regard, both compounds exhibited high permeability with values below 0.1.

The influence of P-glycoprotein (P-gp), a significant efflux transporter, was also examined. The compounds were predicted to be neither substrates nor inhibitors of P-gp. This suggests they would not be actively pumped out of cells by P-gp and would not interfere with the transport of other drugs, potentially leading to increased bioavailability and enhanced therapeutic effects.

Furthermore, with logBB values below -1, the compounds showed poor distribution to the brain. This finding implies a low risk of central nervous system effects and toxicity, which aligns with established pharmacokinetic guidelines.

Assessing how a compound affects metabolic enzymes is a key step in drug development. In this study, an *in silico* analysis of the compounds' interaction with the cytochrome P450 (CYP450) enzyme superfamily-a major player in drug metabolism-was performed. The results predicted that neither compound would inhibit the activity of any CYP450 enzymes,

with the sole exception of compound 1, which was predicted to inhibit CYP1A2. Inhibition of CYP1A2 could suggest a potential risk of hepatotoxicity in some individuals. Additionally, neither compound was predicted to be a substrate for any of the tested CYP450 enzymes.

In drug development, assessing a compound's effect on renal clearance is crucial. The organic cation transporter 2 (OCT2), a key renal uptake transporter, plays a significant role in the disposition of drugs and other compounds. As substrates for OCT2 can be susceptible to adverse interactions with co-administered inhibitors, it is important to evaluate this parameter. In this study, neither of the compounds was predicted to be an OCT2 substrate, nor were they projected to induce hepatotoxicity or skin sensitization.

Toxicity evaluations indicated that compound 1 showed potential carcinogenicity in rats but not in mice. Mutagenicity was also assessed through *in silico* Ames testing, a standard method for determining a compound's potential to cause mutations. This test uses various strains of *Salmonella typhimurium*-such as TA100_10RLI, TA100_NA, TA1523_10RLI and TA1535_NA and can be performed with or without the S9 fraction, which simulates metabolic activation. The TA100 strain is used to detect substances that cause guanine-cytosine base pair substitutions, while the TA1535 strain identifies substances that induce methylation and guanine-cytosine base pair replacements. Based on these predictions, only compound 1 was identified as a potential mutagen in the TA100_NA strain, but it was not predicted to be mutagenic in any of the other strains tested.

Finally, the potential for cardiotoxicity was assessed by evaluating the compounds' inhibition of the human etherago-go-related gene (hERG) channel. Both compounds demonstrated no significant risk of hERG inhibition. The hERG gene encodes Kv11.1, the α -subunit of a potassium ion channel that is critical for cardiac electrical activity. This channel mediates the repolarizing current lkr, which is essential for coordinated cardiac repolarization. While the compounds showed no predicted risk of hERG inhibition, the potential to influence cardiac action potential, particularly in individuals with pre-existing cardiovascular conditions, necessitates further investigation. Therefore, comprehensive toxicological studies are crucial to fully establish the safety profiles of these compounds beyond their traditional uses and to determine their suitability for clinical application.

CONCLUSION

This study successfully isolated and identified quercetin and isoquercetin from *Streptomyces griseoaurantiacus* HNF214, an actinomycete found in *Apis florea* beehives. These

compounds demonstrated antibacterial activity against Grampositive bacteria and exhibited promising cytotoxic effects against human breast, cervical and hepatocellular cancer cell lines, with lower toxicity to normal cells. Molecular docking and *in vitro* assays suggest they inhibit cancer cell growth by downregulating the MAPK/ERK pathway. While *in silico* ADMET predictions indicate generally favorable pharmacokinetic profiles, some potential toxicity concerns were identified, highlighting the need for further comprehensive *in vivo* studies to validate their therapeutic potential and ensure safety.

SIGNIFICANCE STATEMENT

This study discovered the bioactive compounds quercetin and isoquercetin, derived from Streptomyces griseoaurantiacus HNF214 isolated from Apis florea beehives, that can be beneficial for developing novel antibacterial and anticancer agents. These compounds exhibited selective antibacterial effects against Gram-positive pathogens and potent cytotoxicity against breast, cervical and hepatocellular cancer cells. Molecular analysis indicated that their anticancer activity is mediated through inhibition of the MAPK/ERK signaling pathway. The findings suggest that microbial communities in beehives are an underexplored source of pharmaceutically significant metabolites. This study will help the researchers to uncover the critical areas of natural product drug discovery from unique ecological niches that many researchers were not able to explore. Thus, a new theory on hive-associated actinomycetes as therapeutic sources may be arrived at.

ACKNOWLEDGMENT

This work was supported by a research grant (No. SRIF-JRG-2568-08) from the Faculty of Science, Silpakorn University, Nakhon Pathom, Thailand.

REFERENCES

- Selim, M.S.M., S.A. Abdelhamid and S.S. Mohamed, 2021. Secondary metabolites and biodiversity of actinomycetes. J. Genet. Eng. Biotechnol., Vol. 19. 10.1186/s43141-021-00156-9.
- Promnuan, Y., T. Kudo and P. Chantawannkul, 2009. Actinomycetes isolated from beehives in Thailand. World J. Microbiol. Biotechnol., 25: 1685-1689.
- Madden, A.A., A. Grassetti, J.A.N. Soriano and P.T. Starks, 2013. Actinomycetes with antimicrobial activity isolated from paper wasp (Hymenoptera: Vespidae: Polistinae) nests. Environ. Entomol., 42: 703-710.

- Kim, D.R., G. Cho, C.W. Jeon, D.M. Weller, L.S. Thomashow, T.C. Paulitz and Y.S. Kwak, 2019. A mutualistic interaction between Streptomyces bacteria, strawberry plants and pollinating bees. Nat. Commun., Vol. 10. 10.1038/s41467-019-12785-3.
- Khan, K.A., A.A. Al-Ghamdi, H.A. Ghramh, M.J. Ansari and H. Ali *et al.*, 2020. Structural diversity and functional variability of gut microbial communities associated with honey bees. Microb. Pathogen., Vol. 138. 10.1016/j.micpath.2019.103793.
- Grubbs, K.J., D.S. May, J.A. Sardina, R.K. Dermenjian and T.P. Wyche et al., 2021. Pollen Streptomyces produce antibiotic that inhibits the honey bee pathogen Paenibacillus larvae. Front. Microbiol., Vol. 12. 10.3389/fmicb.2021.632637.
- Santos-Beneit, F., A. Ceniceros, A. Nikolaou, J.A. Salas and J. Gutierrez-Merino, 2022. Identification of antimicrobial compounds in two *Streptomyces* sp. strains isolated from beehives. Front. Microbiol., Vol. 13. 10.3389/fmicb.2022.742168.
- 8. Promnuan, Y., S. Promsai, W. Pathom-Aree and S. Meelai, 2021. *Apis andreniformis* associated actinomycetes show antimicrobial activity against black rot pathogen (*Xanthomonas campestris* pv. *campestris*). PeerJ, Vol. 9. 10.7717/peerj.12097.
- 9. de Simeis, D. and S. Serra, 2021. *Actinomycetes*: A never-ending source of bioactive compounds-An overview on antibiotics production. Antibiotics, Vol. 10. 10.3390/antibiotics10050483.
- 10. Shirling, E.B. and D. Gottlieb, 1966. Methods for characterization of *Streptomyces* species. Int. J. Syst. Bacteriol., 16: 313-340.
- Taechowisan, T., N. Mungchukeatsakul and W.S. Phutdhawong, 2018. Antimicrobial resistance pattern of *Staphylococcus aureus* strains isolated from clinical and hospital environment specimens and their correlation with PCR-based approaches. Res. J. Microbiol., 13: 100-118.
- Hockett, K.L. and D.A. Baltrus, 2017. Use of the soft-agar overlay technique to screen for bacterially produced inhibitory compounds. J. Visualized Exp., Vol. 119. 10.3791/55064.
- 13. Cassarini, M., C. Rémond, E. Mühle, D. Clermont and L. Besaury, 2022. *Streptomyces durocortorensis* sp. nov., isolated from oak rhizosphere. Int. J. Syst. Evol. Microbiol., Vol. 72. 10.1099/ijsem.0.005480.
- 14. Taechowisan, T., W. Puckdee and W.S. Phutdhawong, 2019. *Streptomyces zerumbet*, a novel species from *Zingiber zerumbet* (L.) Smith and isolation of its bioactive compounds. Adv. Microbiol., 9: 194-219.
- 15. Jesionek, W., Á.M. Móricz, Á. Alberti, P.G. Ott, B. Kocsis, G. Horváth and I.M. Choma, 2015. TLC-direct bioautography as a bioassay guided method for investigation of antibacterial compounds in *Hypericum perforatum* L. J. AOAC Int., 98: 1013-1020.

- Becker, B., M.P. Lechevalier, R.E. Gordon and H.A. Lechevalier, 1964. Rapid differentiation between *Nocardia* and *Streptomyces* by paper chromatography of whole-cell hydrolysates. Appl. Microbiol., 12: 421-423.
- 17. Boone, C.J. and L. Pine, 1968. Rapid method for characterization of actinomycetes by cell wall composition. Appl. Microbiol., 16: 279-284.
- Castillo, U.F., G.A. Strobel, E.J. Ford, W.M. Hess and H. Porter et al., 2002. Munumbicins, wide-spectrum antibiotics produced by Streptomyces NRRL 30562, endophytic on Kennedia nigriscans. Microbiology, 148: 2675-2685.
- Nakajima, Y., V. Kitpreechavanich, K.I. Suzuki and T. Kudo, 1999. *Microbispora corallina* sp. nov., a new species of the genus *Microbispora* isolated from Thai soil. Int. J. Syst. Evol. Microbiol., 49: 1761-1767.
- 20. Tamura, K., G. Stecher and S. Kumar, 2021. MEGA11: Molecular evolutionary genetics analysis version 11. Mol. Biol. Evol., 38: 3022-3027.
- Pfaller, M.A., R.N. Jones, D.H. Walter and Q.C.S. Group, 2001. Proposed quality control guidelines for National Committee for Clinical Laboratory Standards Susceptibility Tests using the veterinary antimicrobial agent tiamulin. Diagn. Microbiol. Infect. Dis., 40: 67-70.
- 22. van Meerloo, J., G.J.L. Kaspers and J. Cloos, 2011. Cell Sensitivity Assays: The MTT Assay. In: Cancer Cell Culture: Methods and Protocols, Cree, I.A. (Ed.), Humana Press, Totowa, New Jersey, United States, ISBN: 978-1-61779-079-9, pp: 237-245.
- AlZahrani, W.M., S.A. AlGhamdi, S.S. Sohrab and M. Rehan, 2023. Investigating a library of flavonoids as potential inhibitors of a cancer therapeutic target MEK2 using *in silico* methods. Int. J. Mol. Sci., Vol. 24. 10.3390/ijms24054446.
- Gopikrishnan, V., M. Radhakrishnan, T. Shanmugasundaram,
 R. Pazhanimurugan and R. Balagurunathan, 2016.
 Antibiofouling potential of quercetin compound from marine-derived actinobacterium, *Streptomyces fradiae* PE7 and its characterization. Environ. Sci. Pollut. Res., 23: 13832-13842.
- Azeem, M., M. Hanif, K. Mahmood, N. Ameer, F.R.S. Chughtai and U. Abid, 2023. An insight into anticancer, antioxidant, antimicrobial, antidiabetic and anti-inflammatory effects of quercetin: A review. Polym. Bull., 80: 241-262.
- 26. Li, Y., J. Yao, C. Han, J. Yang and M.T. Chaudhry *et al.*, 2016. Quercetin, inflammation and immunity. Nutrients, Vol. 8. 10.3390/nu8030167.
- 27. Yi, H., H. Peng, X. Wu, X. Xu and T. Kuang *et al.*, 2021. The therapeutic effects and mechanisms of quercetin on metabolic diseases: Pharmacological data and clinical evidence. Oxid. Med. Cell. Longevity, Vol. 2021. 10.1155/2021/6678662.

- 28. Almatroodi, S.A., M.A. Alsahli, A. Almatroudi, A.K. Verma and A. Aloliqi *et al.*, 2021. Potential therapeutic targets of quercetin, a plant flavonol, and its role in the therapy of various types of cancer through the modulation of various cell signaling pathways. Molecules, Vol. 26. 10.3390/molecules26051315.
- Sholkamy, E.N., M.S. Ahmed, M.M. Yasser and A.A. Mostafa, 2020. Antimicrobial quercetin 3-O-glucoside derivative isolated from *Streptomyces antibioticus* strain ess_amA8.
 J. King Saud Univ. Sci., 32: 1838-1844.
- 30. Lima, J.V.L., S.C.S. Martins, K.A. de Siqueira, M.A. Soares and C.M. Martins, 2017. Characterization of actinobacteria from the semiarid region, and their antagonistic effect on strains of rhizobia. Afr. J. Biotechnol., 16: 499-507.
- 31. Prashanthi, K., S. Suryan and K.N. Varalakshmi, 2015. *In vitro* anticancer property of yellow pigment from *Streptomyces griseoaurantiacus* JUACT 01. Braz. Arch. Biol. Technol., 58: 869-876.
- Nguyen, T.L.A. and D. Bhattacharya, 2022.
 Antimicrobial activity of quercetin: An approach to its mechanistic principle. Molecules, Vol. 27. 10.3390/molecules27082494.
- 33. Cushnie, T.P.T. and A.J. Lamb, 2005. Antimicrobial activity of flavonoids. Int. J. Antimicrob. Agents, 26: 343-356.
- 34. Abdur Rauf, M. Imran, I.A. Khan, Mujeeb-ur-Rehman, S.A. Gilani, Z. Mehmood and M.S. Mubarak, 2018. Anticancer potential of quercetin: A comprehensive review. Phytother. Res., 32: 2109-2130.
- 35. Abotaleb, M., S.M. Samuel, E. Varghese, S. Varghese, P. Kubatka, A. Liskova and D. Büsselberg, 2019. Flavonoids in cancer and apoptosis. Cancers, Vol. 11. 10.3390/cancers11010028.
- 36. Batra, P. and A.K. Sharma, 2013. Anti-cancer potential of flavonoids: Recent trends and future perspectives. 3 Biotech, 3: 439-459.
- 37. Kopustinskiene, D.M., V. Jakstas, A. Savickas and J. Bernatoniene, 2020. Flavonoids as anticancer agents. Nutrients, Vol. 12. 10.3390/nu12020457.
- 38. Wijaya, S.J., A. Yanuar, R. Handayani and R.R. Syahdi, 2019. *In silico* analysis of flavonoid glycosides and its aglycones as reverse transcriptase inhibitor. Pharmacogn. J., 11: 1252-1255.
- da Silva, F.M.A., K.P.A. da Silva, L.P.M. de Oliveira, E.V. Costa and H.H.F. Koolen *et al.*, 2020. Flavonoid glycosides and their putative human metabolites as potential inhibitors of the SARS-CoV-2 main protease (Mpro) and RNA-dependent RNA polymerase (RdRp). Memórias Inst. Oswaldo Cruz, Vol. 115. 10.1590/0074-02760200207.
- Pan, H.C., Q. Jiang, Y. Yu, J.P. Mei, Y.K. Cui and W.J. Zhao, 2015. Quercetin promotes cell apoptosis and inhibits the expression of MMP-9 and fibronectin via the AKT and ERK signalling pathways in human glioma cells. Neurochem. Int., 80: 60-71.

- 41. Soofiyani, S.R., K. Hosseini, H. Forouhandeh, T. Ghasemnejad and V. Tarhriz *et al.*, 2021. Quercetin as a novel therapeutic approach for lymphoma. Oxid. Med. Cell. Longevity, Vol. 2021. 10.1155/2021/3157867.
- 42. Pires, D.E.V., T.L. Blundell and D.B. Ascher, 2015. pkCSM: Predicting small-molecule pharmacokinetic and toxicity properties using graph-based signatures. J. Med. Chem., 58: 4066-4072.
- 43. Daina, A., O. Michielin and V. Zoete, 2017. SwissADME: A free web tool to evaluate pharmacokinetics, drug-likeness and medicinal chemistry friendliness of small molecules. Sci. Rep., Vol. 7. 10.1038/srep42717.
- 44. Adido, H.E.F., C.K.S. Chagas, G.G. Ferreira, M.L.C. Bastos and M.F. Dolabela, 2023. *In silico* studies on cytotoxicity and antitumoral activity of acetogenins from *Annona muricata* L. Front. Chem., Vol. 11. 10.3389/fchem.2023.1316779.